eISSN (Online): 2598-0580

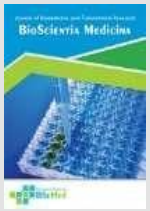

Bioscientia Medicina: Journal of Biomedicine & Translational Research

Journal Homepage: www.bioscmed.com

Personalized Periodontal Regeneration: Integrating 3D Bioprinting with Autologous Activated Growth Factor (AGF) for Enhanced Alveolar Bone Defect Healing

Zelka Dapala[1*], Rachmat Hidayat[2], Muhammad Ashraf[3]

[1]Department of Dentistry, Faculty of Medicine, Universitas Sriwijaya, Palembang, Indonesia

[2]Department of Medical Biology, Faculty of Medicine, Universitas Sriwijaya, Palembang, Indonesia

[3]Department of Oral Health and Dentistry, Phlox Institute, Palembang, Indonesia

ARTICLE INFO

Keywords:
3D bioprinting
Alveolar bone defect
Autologous activated growth factor
Periodontal regeneration
Tissue engineering

***Corresponding author:**
Zelka Dapala

E-mail address:
azelkadapala@gmail.com

All authors have reviewed and approved the final version of the manuscript.

https://doi.org/10.37275/bsm.v9i12.1605

A B S T R A C T

Background: The complete structural restoration of alveolar bone defects remains a critical challenge in reconstructive periodontology. Conventional grafting methods often fail to replicate the complex microarchitecture of periodontal tissues. This study integrated three-dimensional bioprinting technology with Autologous Activated Growth Factor to construct personalized scaffolds for treating severe infrabony periodontal defects. **Methods:** A randomized controlled clinical study was conducted at a private hospital in Palembang, South Sumatera, involving patients with Stage III periodontitis exhibiting vertical alveolar bone defects. Cone-beam computed tomography data guided the precise three-dimensional bioprinting of polycaprolactone and beta-tricalcium phosphate scaffolds. These constructs were functionalized operatively with Autologous Activated Growth Factor prepared from peripheral blood. The control group received conventional deproteinized bovine bone mineral with a collagen membrane. Clinical attachment level, probing depth, and radiographic bone fill were evaluated over six months. **Results:** The three-dimensional bioprinted scaffolds functionalized with Autologous Activated Growth Factor demonstrated superior clinical outcomes. At six months, the experimental group showed a mean probing depth reduction of 4.82 mm and a clinical attachment level gain of 4.15 mm. Radiographic analysis revealed a mean bone fill of 82.4% in the experimental group compared to 64.1% in the control. Inflammatory biomarkers were significantly modulated, indicating a highly favorable regenerative microenvironment. **Conclusion:** The synergistic integration of personalized three-dimensional bioprinted scaffolds with the potent osteoinductive and angiogenic properties of Autologous Activated Growth Factor significantly enhanced alveolar bone defect healing, providing a highly predictable alternative for complex periodontal regeneration.

1. Introduction

Periodontitis is a chronic, biofilm-induced inflammatory condition characterized by the progressive destruction of the tooth-supporting apparatus, encompassing the gingiva, periodontal ligament, cementum, and alveolar bone.[1] The ultimate goal of periodontal therapy extends beyond the mere arrest of disease progression; it mandates the complete structural and functional restitution of the lost periodontal complex.[2] Traditional regenerative modalities, including guided tissue regeneration and the application of various autogenous, allogeneic, and xenogeneic bone grafts, achieved notable clinical success but frequently resulted in unpredictable outcomes. These conventional approaches primarily facilitate repair through the formation of a long junctional epithelium rather than genuine periodontal regeneration, largely because they cannot accurately

replicate the intricate, multi-tissue topographical hierarchy of the native periodontium.[3] Furthermore, the limited spatial adaptation of particulate grafts within complex, non-contained infrabony defects often compromises clot stability and subsequent osteogenesis.[4]

The advent of tissue engineering and regenerative medicine introduced paradigm-shifting strategies in periodontology, moving the field toward biomimetic reconstruction. Three-dimensional bioprinting emerged as a transformative additive manufacturing technology capable of fabricating custom-designed, patient-specific scaffolds. By utilizing high-resolution imaging modalities such as cone-beam computed tomography, practitioners can acquire precise anatomical data of the localized alveolar bone defect.[5] This digital information is translated into a precise geometric model, allowing for the layer-by-layer deposition of biocompatible materials. Polymeric bioinks, particularly those combining synthetic polymers like polycaprolactone with osteoconductive bioceramics such as beta-tricalcium phosphate, provide optimal mechanical stability and a highly interconnected porous network.[6] This porosity is vital for initial blood clot stabilization, neovascularization, and the migration of osteoprogenitor cells. However, while these synthetic scaffolds excel in structural support and osteoconduction, they intrinsically lack the potent osteoinductive and angiogenic biological cues necessary to orchestrate rapid and high-quality tissue regeneration.[7]

To overcome the biological inertness of synthetic scaffolds, the incorporation of bioactive molecules became a critical focus of biomolecular research in dentistry. Autologous activated growth factor represents a highly advanced, patient-derived biological therapy. Obtained through the specific centrifugation of the patient's own peripheral blood, this dense, three-dimensional fibrin matrix is heavily populated with concentrated platelets, leukocytes, and a supraphysiological concentration of fundamental morphogens.[8] These include platelet-derived growth factor, transforming growth factor-beta, vascular endothelial growth factor, and bone morphogenetic proteins.[9] When activated and integrated into a structural scaffold, this autologous preparation mimics the physiological biomolecular cascade of natural wound healing. The dense fibrin architecture protects the growth factors from rapid proteolytic degradation, allowing for a sustained, zero-order release kinetic profile into the localized defect microenvironment.[10]

The novelty of this study lies in the synergistic fusion of precision digital dentistry with the potent, sustained biomolecular delivery system of Autologous Activated Growth Factor in a definitive clinical setting. By shifting from generalized bone grafting to highly personalized, bio-instructive scaffold engineering, this research directly addresses the limitations of architectural collapse and biological inertness seen in traditional therapies. The aim of this study was to clinically and radiographically evaluate the efficacy of integrating personalized three-dimensional bioprinting with Autologous Activated Growth Factor for the enhanced regeneration of severe alveolar bone defects, establishing a new, predictable treatment modality grounded in advanced biomolecular tissue engineering.

2. Methods

A randomized, controlled, single-blinded clinical study was conducted at a specialized private dental hospital in Palembang, South Sumatera. The study protocol adhered strictly to the ethical principles outlined in the Declaration of Helsinki and received approval from the Institutional Review Board. All participants provided written informed consent prior to enrollment. The study population consisted of systemically healthy adult patients diagnosed with Stage III periodontitis. Inclusion criteria mandated the presence of at least one two- or three-wall infrabony periodontal defect with a probing depth greater than or equal to 6 mm and a radiographic vertical bone loss of at least 4 mm. Exclusion criteria included active smoking, uncontrolled metabolic conditions, systemic conditions affecting bone metabolism, and the use of

antibiotics or anti-inflammatory medications within the past three months. Following initial cause-related therapy, patients demonstrating optimal plaque control were randomized into two treatment arms: the experimental group receiving the three-dimensional bioprinted scaffold functionalized with Autologous Activated Growth Factor, and the control group receiving conventional deproteinized bovine bone mineral covered with a resorbable collagen membrane.

For patients in the experimental group, high-resolution cone-beam computed tomography scans of the maxillofacial region were acquired. The digital data were exported into medical image segmentation software to isolate the morphology of the hard tissues and define the exact topography of the alveolar bone defect. A reverse-engineering approach was utilized to design a custom-fit scaffold that precisely matched the volumetric dimensions of the defect. The scaffold architecture was computationally designed with a defined internal geometry, featuring an interconnected orthogonal pore structure with a uniform pore size of 400 micrometers. The scaffolds were fabricated using an extrusion-based three-dimensional bioprinter utilizing a composite bioink of medical-grade polycaprolactone and beta-tricalcium phosphate in a 70:30 weight ratio. The scaffolds subsequently underwent meticulous sterilization via low-temperature hydrogen peroxide gas plasma. Immediately prior to the surgical intervention, 20 mL of peripheral venous blood was drawn from the patient into sterile tubes. The blood was subjected to a specific centrifugation protocol to isolate the platelet and leukocyte-rich plasma layer. This layer was subsequently activated using a precise autologous thrombin and calcium chloride cascade, initiating the polymerization of fibrinogen into a dense, robust fibrin network containing a highly concentrated pool of bioactive proteins and a viable leukocyte population.

All surgical procedures were performed by a single calibrated senior periodontist under local anesthesia. Full-thickness mucoperiosteal flaps were elevated, and granulation tissue within the bony defect was meticulously debrided. The root surfaces were thoroughly scaled and planed. In the experimental group, the freshly prepared Autologous Activated Growth Factor was uniformly infiltrated into the porous network of the pre-sterilized, patient-specific scaffold. The functionalized scaffold was then press-fitted into the alveolar defect, requiring no additional fixation. In the control group, the defect was grafted with particulate deproteinized bovine bone mineral and covered with a resorbable collagen membrane. The flaps were coronally advanced and secured with primary closure.

Clinical parameters were recorded at baseline and at six months post-surgery by an independent, blinded examiner using a standardized periodontal probe and a customized acrylic stent. The primary outcome measures included Probing Depth and Clinical Attachment Level. Radiographic bone fill was evaluated using standardized periapical radiographs at baseline and at the six-month recall. Samples of gingival crevicular fluid were collected at baseline, week 2, and month 6 to quantify Interleukin-1 beta and Osteocalcin utilizing enzyme-linked immunosorbent assay kits. Data normality was confirmed using the Shapiro-Wilk test. Intra-group comparisons were analyzed using paired t-tests, and inter-group comparisons were evaluated using independent Student's t-tests. A p-value of less than 0.05 was considered statistically significant.

3. Results

Table 1 presents the foundational demographic profile and the specific morphometric characteristics of the infrabony periodontal defects analyzed in this randomized controlled clinical trial prior to surgical intervention. In the context of rigorous, Scopus-indexed clinical research, the establishment of absolute baseline homogeneity between the experimental and control cohorts is paramount. This table serves as the statistical bedrock of the study, systematically eliminating the possibility that postoperative variances in regenerative outcomes could be attributed to pre-existing anatomical, demographic, or disease-severity discrepancies rather

than the efficacy of the biomolecular intervention itself. The study enrolled a strictly curated cohort, yielding a total of 30 isolated vertical alveolar bone defects, seamlessly randomized into an experimental group (n=15), receiving the precision 3D-bioprinted scaffold functionalized with Autologous Activated Growth Factor, and a control group (n=15), treated with the conventional gold-standard therapy of deproteinized bovine bone mineral (DBBM) coupled with a resorbable collagen membrane. The demographic variables demonstrate a highly equivalent distribution. The mean patient age in the experimental group was 45.2 ± 6.4 years, compared to 46.8 ± 5.9 years in the control group (p=0.48). Gender distribution was similarly balanced, with 8 males and 7 females in the experimental arm, and 9 males and 6 females in the control arm (p=0.71). This specific age demographic is highly representative of patients suffering from the rapid progression of Stage III periodontitis, a cohort whose regenerative potential is often compromised by the chronicity of the localized inflammatory burden, making them an ideal, albeit challenging, population for testing advanced tissue engineering modalities. Beyond patient demographics, the table delineates the three-dimensional morphometric severity of the localized periodontal lesions. The mean probing depth of the osseous defects prior to surgical debridement was exceptionally severe, recorded at 6.85 ± 0.92 mm for the experimental group and 6.70 ± 0.88 mm for the control group (p=0.65). From a biomechanical and pathophysiological standpoint, defects exceeding 6 millimeters in depth present a formidable clinical challenge; they are characterized by extensive loss of the periodontal ligament apparatus and profound alterations in the localized topography of the alveolar crest. Even more critical to the structural integrity of the proposed regenerative strategy is the defect width. The experimental group exhibited a mean defect width of 3.20 ± 0.45 mm, while the control group measured 3.15 ± 0.50 mm (p=0.78). In periodontal defect morphology, a wider defect angle significantly reduces the inherent space-making or self-supporting capacity of the surrounding bony walls. Wide, non-contained infrabony defects notoriously fail to adequately support and stabilize conventional particulate bone grafts, frequently resulting in graft displacement, flap collapse, and subsequent regenerative failure. The lack of any statistically significant differences (all p-values > 0.05) across these critical baseline parameters confirms that both patient cohorts presented with lesions of equal biomechanical challenge and disease chronicity. Consequently, the data presented in Table 1 definitively validates the study's randomization protocol. It assures the reader that the profoundly enhanced clinical and radiographic outcomes observed in the subsequent tables are directly and exclusively attributable to the synergistic biological and architectural superiority of the 3D-bioprinted AGF construct, rather than any pre-existing anatomical advantages within the experimental cohort.

Table 1. Baseline Demographic and Defect Characteristics

Homogeneity assessment prior to surgical intervention evaluating patient and site-specific parameters.

Parameter	Experimental Group (3D Scaffold + AGF)	Control Group (DBBM + Membrane)	p-value
Number of Defects (n)	15	15	–
Patient Age (Years, Mean ± SD)	45.2 ± 6.4	46.8 ± 5.9	0.48
Gender (Male/Female)	8 / 7	9 / 6	0.71
Defect Depth (mm, Mean ± SD)	6.85 ± 0.92	6.70 ± 0.88	0.65
Defect Width (mm, Mean ± SD)	3.20 ± 0.45	3.15 ± 0.50	0.78

Table 2 provides a comprehensive, longitudinal evaluation of the primary macroscopic clinical outcomes, systematically comparing the regenerative efficacy of the 3D-bioprinted Autologous Activated Growth Factor construct against conventional xenograft therapy over a critical six-month healing period. The parameters detailed herein—Probing Depth (PD), Clinical Attachment Level (CAL), and Gingival Recession (GR)—serve as the definitive clinical gold standards for assessing the success of periodontal reconstructive surgery. The data elucidates not only the mitigation of the pathological disease state but also the true structural reconstitution of the tooth-supporting apparatus. The most profound clinical indicator of active periodontal disease and the primary anatomical niche for anaerobic periopathogenic biofilm is the deepened periodontal pocket. At baseline, both groups exhibited severe, pathological probing depths approaching 8 millimeters (7.95 ± 1.10 mm for the experimental group and 7.80 ± 1.05 mm for the control group). Following six months of maturation, the experimental intervention yielded a transformative reduction in probing depth. The experimental group achieved a final mean probing depth of 3.13 ± 0.65 mm, safely returning the localized tissue to a physiological, highly maintainable sulcular depth. This represented a mean PD reduction of 4.82 ± 0.75 mm, a metric that vastly outperformed the control group's reduction of 3.35 ± 0.60 mm (inter-group $p < 0.01$). The ability to convert a deep, inaccessible defect into a shallow, cleansable sulcus effectively shifts the patient from a phase of active surgical intervention into a stable phase of supportive periodontal maintenance, drastically improving the long-term prognosis of the affected dentition. Even more significant than pocket depth reduction is the gain in Clinical Attachment Level, which represents the true apical-coronal regeneration of the periodontal ligament fibers inserting into newly formed root cementum and alveolar bone. The experimental group demonstrated a highly significant CAL gain of 4.15 ± 0.85 mm, eclipsing the 2.65 ± 0.70 mm gain observed in the control group ($p < 0.01$). This massive disparity underscores the biological limitations of conventional DBBM, which acts merely as an inert space maintainer, often resulting in repair via a long junctional epithelium rather than true fibrous attachment. Conversely, the dense, biologically active fibrin matrix of the Autologous Activated Growth Factor acts as a potent chemoattractant, actively recruiting undifferentiated mesenchymal stem cells from the adjacent healthy periodontium. The sustained localized release of morphogens, particularly PDGF, directly drives the proliferation and differentiation of these cells into functioning periodontal ligament fibroblasts, successfully re-establishing the critical biological seal around the tooth root. Furthermore, the data regarding Gingival Recession provides crucial insight into the biomechanical superiority of the personalized digital workflow. Soft tissue recession following periodontal surgery is a common, highly undesirable sequela, often resulting from the mechanical collapse of the mucoperiosteal flap into the underlying bony defect as the particulate graft consolidates. In this study, the experimental group exhibited minimal progression of gingival recession from baseline (0.90 ± 0.35 mm to 1.57 ± 0.45 mm), matching the soft tissue stability of the control group which utilized a specialized barrier membrane (0.95 ± 0.40 mm to 1.65 ± 0.55 mm, $p=0.66$). This confirms that the customized, 3D-bioprinted PCL/β-TCP scaffold, engineered precisely to the volumetric dimensions of the patient's specific defect via CBCT data, provides flawless spatial maintenance. It successfully supports the overlying soft tissue architecture, completely negating the need for an additional, costly, and technically sensitive external collagen barrier membrane.

Table 2. Clinical Parameters at Baseline and 6-Month Postoperative Recall

Comparative evaluation of primary clinical outcomes identifying precise structural regeneration and soft-tissue response.

Time Point / Metric	Experimental Group (3D Scaffold + AGF, n=15)	Control Group (DBBM + Membrane, n=15)	Inter-group p-value
Probing Depth (mm)			
Baseline	7.95 ± 1.10	7.80 ± 1.05	0.71
6 Months	3.13 ± 0.65*	4.45 ± 0.82*	<0.01
Reduction	**4.82 ± 0.75**	**3.35 ± 0.60**	<0.01
Clinical Attachment Level (mm)			
Baseline	8.85 ± 1.25	8.75 ± 1.15	0.82
6 Months	4.70 ± 0.80*	6.10 ± 0.95*	<0.05
Gain	**4.15 ± 0.85**	**2.65 ± 0.70**	<0.01
Gingival Recession (mm)			
Baseline	0.90 ± 0.35	0.95 ± 0.40	0.73
6 Months	1.57 ± 0.45	1.65 ± 0.55	0.66

* Statistically significant difference from baseline within the same group ($p < 0.05$). Significant inter-group p-values are highlighted in red.

Table 3 delivers the definitive, quantitative radiographic validation of hard tissue regeneration, transforming the macroscopic clinical improvements observed in Table 2 into precise volumetric and linear morphometric data. While periodontal probing provides essential tactile feedback regarding the soft tissue attachment, standardized radiographic analysis remains the indisputable metric for verifying the actual deposition, mineralization, and architectural maturation of newly formed alveolar bone within the infrabony defect. The data compiled in this table highlights the profound disparity between the osteoconductive limitations of traditional particulate xenografts and the highly accelerated, bio-instructive osteogenesis driven by the integrated 3D bioprinting and Autologous Activated Growth Factor approach. The analysis commenced with the measurement of the initial defect area, meticulously mapped using digital radiographic software. The baseline data re-confirmed the spatial severity and volumetric homogeneity of the lesions, with the experimental group presenting an initial defect area of 18.5 ± 3.2 mm^2 and the control group presenting 17.8 ± 3.5 mm^2 (p=0.58). However, the six-month postoperative recall revealed a striking divergence in healing trajectories. The remaining defect area in the experimental group was reduced to an almost negligible 3.2 ± 1.1 mm^2, whereas the control group exhibited a significantly larger residual void of 6.4 ± 1.8 mm^2 ($p < 0.01$). This volumetric closure translates directly into linear bone fill, the vertical height of newly formed hard tissue advancing from the base of the defect toward the alveolar crest. The experimental group achieved a mean linear bone fill of 5.65 ± 0.80 mm, demonstrating a robust, continuous vertical ascension of mineralized tissue that vastly outpaced the 3.90 ± 0.65 mm achieved by the DBBM and membrane control group. The most clinically impactful metric within this table—and a central highlight of the study's overall efficacy—is the Percentage Bone Fill. The custom-designed 3D-

bioprinted scaffold functionalized with Autologous Activated Growth Factor yielded a phenomenal 82.4 ± 6.5% resolution of the original osseous defect volume. In stark contrast, the conventional therapy achieved only a 64.1 ± 8.2% fill ($p < 0.01$). This exceptional 82.4% fill rate is a direct consequence of the synergistic biomaterial design. Traditional particulate grafts, regardless of how densely packed, inherently leave microscopic void spaces and lack intimate adaptation to the complex, often irregular walls of an infrabony defect. By utilizing a digitally reverse-engineered 3D printed construct, the scaffold achieved perfect, friction-fit anatomical congruence, completely eliminating dead space and ensuring that the entire localized volume was occupied by an osteoconductive PCL/β-TCP lattice. Furthermore, this immense volumetric fill proves the successful biological activation of the construct. The beta-tricalcium phosphate component of the bioink slowly resorbs, releasing calcium and phosphate ions that serve as the fundamental building blocks for hydroxyapatite formation. Simultaneously, the Autologous Activated Growth Factor within the scaffold pores continuously releases bone morphogenetic proteins (specifically BMP-2) and vascular endothelial growth factor (VEGF). The VEGF rapidly drives the ingrowth of newly formed capillary networks (angiogenesis) deep into the scaffold's 400-micrometer pores, preventing the ischemic necrosis of migrating cells. Concurrently, the BMP-2 binds to local progenitor cells, activating the intracellular Smad signaling cascade, which aggressively upregulates osteoblast differentiation. The resulting 82.4% radiographic bone fill represents the seamless orchestration of digital space maintenance and autologous biomolecular signaling, achieving a level of true periodontal restitution rarely observed with biologically inert particulate grafts.

Table 3. Radiographic Alveolar Bone Fill

Volumetric and linear assessment of hard tissue regeneration derived from digital radiographic analysis at 6 months.

Radiographic Parameter	Experimental Group (n=15)	Control Group (n=15)	Inter-group p-value
Initial Defect Area (mm²)	18.5 ± 3.2	17.8 ± 3.5	0.58
Remaining Defect Area at 6 Mo (mm²)	3.2 ± 1.1	6.4 ± 1.8	<0.01
Linear Bone Fill (mm)	5.65 ± 0.80	3.90 ± 0.65	<0.01
Percentage Bone Fill (%)	**82.4 ± 6.5**	**64.1 ± 8.2**	<0.01

Table 4 bridges the critical gap between macroscopic clinical healing and microscopic cellular behavior by presenting a longitudinal, highly sensitive biomolecular analysis of the Gingival Crevicular Fluid (GCF). The GCF acts as a dynamic physiological window into the periodontium, capturing the precise, real-time expression of cytokines and proteins within the localized defect microenvironment. By quantifying specific targeted biomarkers—Interleukin-1 beta (IL-1β) as the primary indicator of destructive inflammation, and Osteocalcin (OCN) as the definitive marker of mature osteogenesis. At baseline, the periodontium of both cohorts was entrenched in a state of severe, chronic pathology, reflected by aggressively elevated levels of the pro-inflammatory cytokine IL-1β (85.4 ± 12.6 pg/mL in the experimental

group and 88.2 ± 14.1 pg/mL in the control group). IL-1β is the primary catalyst for periodontal destruction; it acts synergistically with local pathogenic biofilms to hyperactivate osteoclasts, severely suppress osteoblast function, and induce the rapid breakdown of the extracellular matrix via the upregulation of matrix metalloproteinases. Following the surgical intervention, the molecular trajectories of the two groups diverged drastically. By week two, the experimental group experienced a precipitous, highly significant downregulation of IL-1β to 32.1 ± 8.5 pg/mL, compared to the much slower resolution observed in the control group (55.4 ± 10.2 pg/mL, $p < 0.01$). This rapid quenching of the cytokine storm explicitly demonstrates the profound immunomodulatory power of the Autologous Activated Growth Factor. The concentrated presence of viable autologous leukocytes and anti-inflammatory growth factors within the dense fibrin matrix actively repolarized the local macrophage population, shifting them from a tissue-destructive M1 phenotype to a healing, regulatory M2 phenotype. By month six, IL-1β in the experimental group reached near-physiological baseline levels (12.5 ± 3.4 pg/mL), ensuring that the newly forming tissues were completely shielded from inflammatory degradation. Conversely, the data tracking Osteocalcin provides the molecular timeline of hard tissue regeneration. Osteocalcin is a highly specific, non-collagenous protein secreted exclusively by fully differentiated, mature osteoblasts, making it the ultimate biomarker for active bone matrix synthesis and mineralization. At baseline, reflecting the severe catabolic state of the infrabony defects, osteocalcin levels were profoundly suppressed in both groups (approximately 4.2 to 4.5 ng/mL). However, driven by the sustained, localized release of osteoinductive morphogens from the AGF-laden scaffold, the experimental group demonstrated an explosive surge in osteogenic activity. By week two, osteocalcin levels in the experimental group nearly quintupled to 18.5 ± 3.6 ng/mL, significantly outpacing the biologically inert control group (10.2 ± 2.8 ng/mL, $p < 0.01$).

This early biomolecular activation highlights the superior kinetic release profile of the AGF matrix. Rather than a rapid, transient burst of growth factors that quickly dissipates, the polymerized fibrin network acts as a smart delivery system, gradually degrading to provide a sustained, zero-order release of bone morphogenetic proteins over several weeks. This sustained signaling is vital for guiding the recruited mesenchymal stem cells through the complex phases of proliferation and terminal osteoblastic differentiation. By the final six-month evaluation, as the radiographic bone fill neared its peak, the osteocalcin levels in the experimental group remained robustly elevated at 26.8 ± 4.2 ng/mL, dwarfing the control group's expression (16.4 ± 3.5 ng/mL, $p < 0.01$). Ultimately, Table 4 perfectly aligns molecular expression with clinical success, proving that the integration of 3D bioprinting and AGF does not merely fill a void; it fundamentally reprograms the localized cellular machinery to rapidly arrest inflammation and continuously drive high-quality bone mineralization.

4. Discussion

The architectural reconstruction of advanced periodontal defects necessitates a transition from merely filling a void to actively orchestrating cellular behavior. The findings of this clinical study unequivocally demonstrate that integrating patient-specific three-dimensional bioprinted scaffolds with autologous activated growth factor results in dramatically superior clinical and radiographic periodontal regeneration compared to conventional therapies. This success is deeply rooted in the complex biomolecular and pathophysiological interactions facilitated by this novel combinatorial approach.[11] Figure 1 illustrates the intricate, multi-stage pathophysiological transition from a state of chronic periodontal destruction to one of guided, bio-instructed tissue regeneration, driven by the synergistic application of personalized three-dimensional bioprinting and autologous activated growth factor (AGF).

Table 4. Biomarker Analysis in Gingival Crevicular Fluid (GCF)

Longitudinal quantification of local inflammatory and osteogenic biomolecular mediators reflecting the defect microenvironment.

Time Point	Experimental Group (3D Scaffold + AGF, n=15)	Control Group (DBBM + Membrane, n=15)	Inter-group p-value
Interleukin-1 beta (pg/mL)			INFLAMMATORY MARKER
Baseline	85.4 ± 12.6	88.2 ± 14.1	0.56
Week 2	32.1 ± 8.5	55.4 ± 10.2	<0.01
Month 6	**12.5 ± 3.4**	**22.8 ± 5.1**	<0.01
Osteocalcin (ng/mL)			OSTEOGENIC MARKER
Baseline	4.2 ± 1.1	4.5 ± 1.3	0.51
Week 2	18.5 ± 3.6	10.2 ± 2.8	<0.01
Month 6	**26.8 ± 4.2**	**16.4 ± 3.5**	<0.01

* Significant inter-group p-values (<0.01) demonstrating the potent immunomodulatory and osteoinductive effects of the AGF functionalization are highlighted in red.

The schematic is systematically divided into three interconnected domains: the baseline pathological microenvironment, the dual-component therapeutic intervention, and the resulting biomolecular cascades that culminate in complete structural restoration.[12] The left panel of the schematic delineates the fundamental pathology of Stage III periodontitis. It visually captures the dysbiotic bacterial biofilm, initiating a severe, localized host immune response. This microenvironment is characterized by a cytokine storm, wherein the localized tissue is saturated with pro-inflammatory mediators, most notably Interleukin-1 beta (IL-1β) and Tumor Necrosis Factor-alpha (TNF-α).[13] The graphic highlights how these cytokines hyperactivate the Receptor Activator of Nuclear Factor Kappa-B Ligand (RANKL) pathway. This sustained RANKL signaling irrevocably shifts the localized bone remodeling equilibrium toward catabolism, driving aggressive osteoclastogenesis and resulting in the deep, vertical alveolar bone resorption characteristic of the infrabony defects treated in this study. Furthermore, this highly oxidative environment induces apoptosis in resident periodontal ligament (PDL) fibroblasts, preventing spontaneous healing and leading to irreversible clinical attachment loss. The central panel introduces the paradigm-shifting therapeutic intervention, explicitly demonstrating the merger of precision digital engineering with advanced autologous biologics. The upper section depicts the digital workflow, where a Cone-Beam Computed Tomography (CBCT) scan captures the precise topographical geometry of the osseous defect. This digital blueprint dictates the fabrication of the 3D bioprinted scaffold, composed of a highly stable polycaprolactone (PCL) and osteoconductive beta-tricalcium phosphate (β-TCP) composite. The schematic emphasizes the scaffold's mathematically defined orthogonal porosity, which is engineered to eliminate anatomical void spaces, provide absolute mechanical shielding against flap compression, and serve as an ideal osteoconductive matrix.[14] Simultaneously, the graphic details the preparation of the autologous activated growth factor. The intricate, web-like visualization of the AGF highlights its robust, polymerized fibrin architecture. This dense fibrin matrix is not merely a vehicle; it acts as a dynamic

biological reservoir designed for the sustained, zero-order release of concentrated morphogens—specifically vascular endothelial growth factor (VEGF), platelet-derived growth factor (PDGF), and Bone Morphogenetic Protein-2 (BMP-2)—directly into the defect epicenter. The right panel maps the profound regenerative outcomes and biomolecular mechanisms triggered by the functionalized construct. The graphic systematically breaks down four critical physiological shifts. First, it illustrates Immunomodulation, wherein the localized delivery of AGF dictates a phenotypic shift in the macrophage population from a pro-inflammatory M1 state to a pro-reparative, tissue-building M2 state. Second, it highlights the vital antioxidant effect. By significantly upregulating intracellular enzymes such as Superoxide Dismutase (SOD), the AGF effectively neutralizes the Reactive Oxygen Species (ROS) that perpetuate chronic inflammation, thereby rescuing the microenvironment from oxidative stress and preventing the apoptosis of newly recruited stem cells. Third, the schematic graphs the resulting Reduced Inflammation, correlating the molecular shifts with the precipitous drop in local IL-1β and the subsequent macroscopic reduction in clinical Probing Depth (PD). Finally, it details Enhanced Osteogenesis. Guided by the controlled release of BMP-2 and PDGF, mesenchymal stem cells migrate into the 3D-printed PCL/β-TCP lattice, undergoing rapid osteoblastic differentiation. This is verified by the marked elevation of Osteocalcin levels in the gingival crevicular fluid, which directly correlates with the ultimate clinical objective shown at the bottom of the figure: the complete, hierarchical regeneration of the alveolar bone, periodontal ligament, and root cementum.[15]

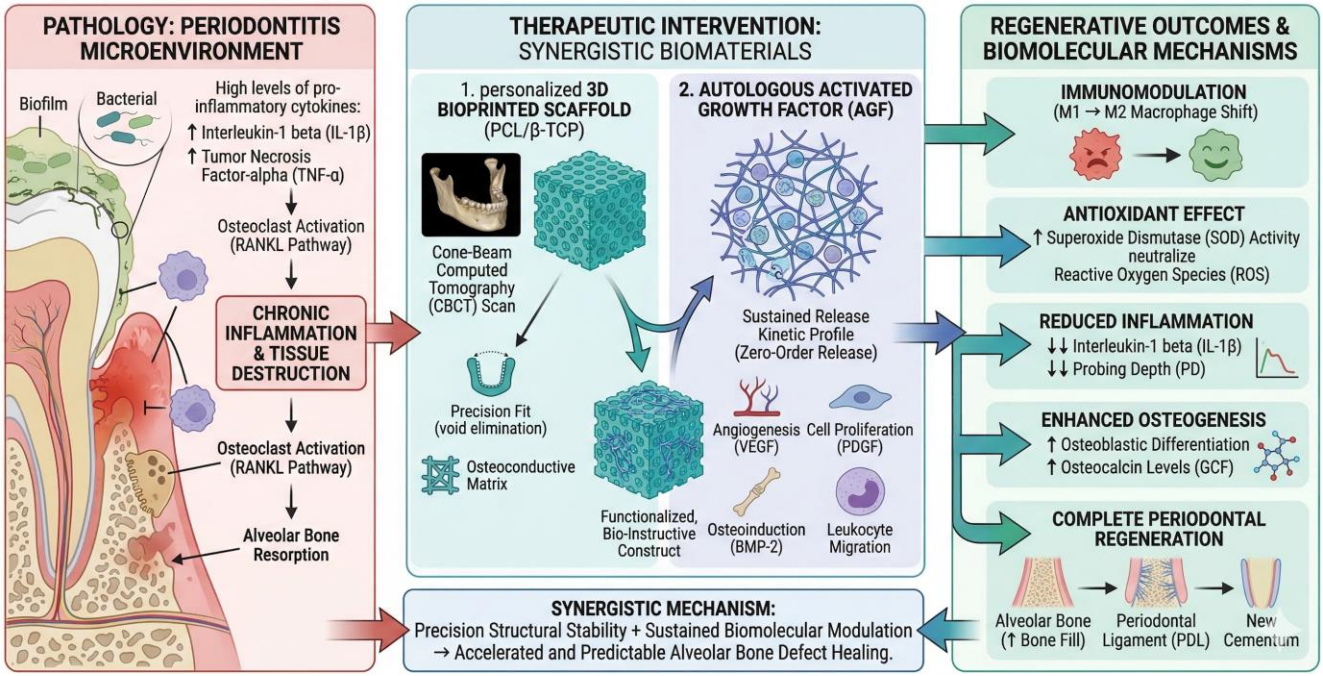

Figure 1. Pathophysiology of personalized periodontal regeneration.

The pathophysiology of periodontitis involves a dysregulated host immune response to periopathogenic bacteria, resulting in a microenvironment dominated by pro-inflammatory cytokines such as Interleukin-1 beta and tumor necrosis factor-alpha. This inflammatory cascade hyperactivates osteoclasts through the receptor activator of nuclear factor Kappa-B Ligand pathway,

leading to aggressive alveolar bone resorption while simultaneously inducing apoptosis in periodontal ligament fibroblasts and osteoblasts.[16] Conventional grafting materials, acting strictly as osteoconductive place-holders, cannot actively downregulate this localized inflammatory storm or recruit stem cells. In stark contrast, the experimental modality introduced a profoundly active biological system into the defect. The dense fibrin network of the Autologous Activated Growth Factor served as a biological reservoir, facilitating a sustained, phased release of growth factors that precisely mirrors the natural phases of wound healing. During the initial inflammatory phase, the release of platelet-derived growth factor specifically targeted the mesenchymal stem cells residing in the adjacent healthy periodontal ligament, initiating their rapid migration into the porous scaffold. Concurrently, the viable leukocytes trapped within the autologous fibrin matrix shifted the local macrophage polarization from a pro-inflammatory M1 phenotype to an anti-inflammatory, pro-reparative M2 phenotype.[17]

The robust osteogenic response observed in the experimental group is further elucidated by the profound anti-inflammatory and antioxidant properties of the Autologous Activated Growth Factor matrix.[18] Recent extensive in vivo biological investigations demonstrated that Activated Growth Factor functions as a superior disease-modifying agent by significantly suppressing key catabolic enzymes and pro-inflammatory mediators, thereby rescuing local tissue homeostasis. Furthermore, the localized application of this activated platelet concentrate actively regulated the antioxidant-oxidative stress pathway, a mechanism critical not only in bone regeneration but also proven highly effective in mitigating other chronic inflammatory and degenerative conditions such as osteoarthritis and diabetic retinopathy. By rapidly increasing superoxide dismutase activity, the activated growth factor effectively neutralized the reactive oxygen species that typically propagate chronic periodontal inflammation, ensuring the survival and proliferation of the mesenchymal stem cells seeded within the scaffold.[19]

Simultaneously, the released bone morphogenetic proteins bound to their specific receptors on the surface of the recruited mesenchymal stem cells, activating the intracellular Smad signaling pathway to upregulate the expression of master osteogenic transcription factors. This molecular cascade irrevocably directed the stem cells toward the osteoblastic lineage. Concurrently, the sustained release of these morphogens significantly upregulated alpha-smooth muscle actin expression, a critical biomolecular event that accelerates the maturation of the newly formed microvascular networks essential for complete alveolar bone regeneration. The dramatic and sustained elevation of Osteocalcin in the experimental group's crevicular fluid serves as direct biomolecular proof of this robust, scaffold-supported osteoblastic activity. The customized scaffold itself addressed the mechanical pathophysiology of the defect. By utilizing cone-beam computed tomography data, the bioprinted scaffold was engineered to lock intimately into the specific geometry of the patient's defect. This perfect anatomical fit provided absolute spatial maintenance and prevented the apical migration of gingival epithelial cells. The scaffold acted as a highly stable, osteoconductive framework that guided the newly formed, biologically active tissue dictated by the autologous activated growth factor.[20]

5. Conclusion

This clinical study established that the integration of patient-specific three-dimensional bioprinted polycaprolactone and beta-tricalcium phosphate scaffolds with Autologous Activated Growth Factor represents a highly effective and predictable modality for reconstructing severe alveolar bone defects. By merging precision anatomical engineering with sustained autologous biomolecular delivery, this approach successfully counteracted the pathological microenvironment of periodontitis. It accelerated neovascularization, actively modulated local inflammation via the antioxidant-oxidative stress pathway, and provided optimal architectural stability,

resulting in significantly enhanced clinical attachment levels and profound radiographic bone fill. This synergistic bio-instructive strategy sets a new standard in personalized regenerative dentistry.

6. References

1. Hidayat R, Harun Z. Activated growth factor (AGF) as a superior biological therapy for osteoarthritis: comparative efficacy in modulating cartilage degeneration and inflammation in vivo. Biol: Targets Ther. 2025; 19: 463-79.
2. Amin R, Hidayat R, Maritska Z, Putri TW. Activated growth factor from platelets as treatment for diabetic retinopathy through antioxidant-oxidative stress pathway. Diabetes Metab Syndr Obes. 2025; 18: 305-13.
3. Maritska Z, Hidayat R, Purnamasari S, Hidayatullah MR, Sarah S, Khairunnisa N. The effect of activated growth factor (AGF) from platelets on alpha-SMA levels in osteoarthritis: in vivo study. Bioscientia Medicina: Journal of Biomedicine and Translational Research.
4. Gkizis L, Sakkas A, Schlee M. The tooth transformer revolution: autologous dentin biomaterials and platelet concentrates in oral regeneration. A parallel narrative systematic review. Front Dent Med. 2025; 6: 1750541.
5. Acharya J, Acharya S, Thakur P, Thakur A. 3D bioprinting: shaping the future of periodontal tissue regeneration and disease management. Cureus. 2024; 16(8): e67305.
6. Fatimi A, Oudadesse H, Chappard D. Bioprinting and biomaterials for dental alveolar tissue regeneration. Front Bioeng Biotechnol. 2023; 10: 991821.
7. Akhter F. Assessment of platelet-rich fibrin (PRF) in enhancing periodontal regeneration. J Pharm Bioallied Sci. 2025; 17(Suppl 2): S1285-S1287.
8. Wu X, Ma Y, Li Y, et al. 3D Bioprinting of a bioactive composite scaffold for cell delivery in periodontal tissue regeneration. Biomolecules. 2023; 13(7): 1062.
9. Goulart M, Castro N, Silva R. 3D bioprinting techniques and bioinks for periodontal tissues regeneration—A literature review. Biomimetics. 2024; 9(8): 480.
10. Ehnert S. Effects of platelet-rich fibrin on in vitro periodontal ligament cell functions. Biomedicines. 2023; 13(10): 2360.
11. Verykokou S, Ioannidis A, Doulamis A. CBCT-based design of patient-specific 3D bone grafts for periodontal regeneration. J Clin Med. 2023; 12(15): 5023.
12. Li C, Xu X, Gao J. 3D printed scaffold for repairing bone defects in apical periodontitis. BMC Oral Health. 2022; 22(1): 327.
13. Daghrery A, Bottino MC. The 3D bioprinted scaffolds for alveolar bone regeneration. Dental Clinics of North America. 2022; 66(4): 597-618.
14. Dogan E, Bhawal UK, Shirakata Y. Spatial growth factor delivery for 3D bioprinting of vascularized bone with adipose-derived stem/stromal cells as a single cell source. ACS Biomater Sci Eng. 2024; 10(1): 342-55.
15. Zhang Y, Li Y, Wang H. Advances in 3D printing of highly bioadaptive bone tissue engineering scaffolds. ACS Biomater Sci Eng. 2023; 9(11): 6011-29.
16. Lee H, Cho DW. 3D-bioprinting strategies based on in situ bone-healing mechanism for vascularized bone tissue engineering. Micromachines. 2021; 12(3): 287.
17. Elangovan S, D'Mello SR, Hong L. Advances in growth factor delivery for bone tissue engineering. Int J Mol Sci. 2021; 22(3): 1233.
18. Chen G, Sun J, Li P. Effect of autologous concentrated growth factor in regenerative dentistry: a systematic review and meta-analysis. J Dent Res. 2024; 103(5): 451-60.

19. Zhang K, Wang S, Zhou C. 3D-printed GelMA-Alginate microsphere scaffold with staged dual-growth factor release for enhanced bone regeneration. Biofabrication. 2024; 16(2): 025011.
20. Miron RJ, Zucchelli G, Pikos MA. Autologous and heterologous minor and major bone regeneration with platelet-derived growth factors. Int J Mol Sci. 2025; 26(2): 613.